Pakistan Veterinary Journal

ISSN: 0253-8318 (PRINT), 2074-7764 (ONLINE)
DOI: 10.29261/pakvetj/2026.196

RESEARCH ARTICLE

Malus toringoides Polysaccharide Alleviates DSS-Induced Colitis in Mice and Is Associated with Gut Microbiota–Metabolite Remodeling and Nrf2/HO-1–NF-κB Signaling

Youying Li[1#], Qinhong Yang[1,2#], Honghui Ren[1], Huikang Wang[1], Bin Fan[1], Zhaobin Xia[1], Wenbin Xu[1], Qian Deng[1], Feng Fan[4], Lishuxin Huang [5*], Jianping Wu[3*] and Wenju Liao[1*]

[1]School of Ecology and Agriculture, Sichuan Minzu College, Kangding 626001, Sichuan Province, China; [2]The Yunnan Key Laboratory of Veterinary Etiological Biology, College of Veterinary Medicine, Yunnan Agricultural University, Kunming 650201, Yunnan Province, China; [3]Animal Husbandry Research Institute, Ganzi Tibetan Autonomous Prefecture, Kangding 626000, Sichuan Province, China; [4]Bureau of Agriculture, Animal Husbandry, Rural Affairs, and Science & Technology of Kangding City, Kangding 626000, Sichuan Province, China; [5]Key Laboratory of Chemistry in Ethnic Medicinal Resources, State Ethnic Affairs Commission & Ministry of Education, School of Ethnic Medicine, Yunnan Minzu University, Kunming 650504, Yunnan Province, China.
[#]These authors contributed equally to this article
*Corresponding author: huanglishuxin19@163.com (LH); 18011279956@163.com (JW) ; wenjuliao@126.com (WL)

ARTICLE HISTORY (26-860)

Received: July 12, 2026
Revised: August 20, 2026
Accepted: August 22, 2026
Published online: August 24, 2026

Key words:
Malus toringoides
polysaccharide
Ulcerative colitis
Gut microbiota
Fecal metabolomics
Intestinal barrier

ABSTRACT

Plant polysaccharides have garnered an increasing amount of attention as potential natural candidates for enhancing intestinal health in animals. The protective effects of *Malus toringoides* polysaccharide (MTK) against dextran sulphate sodium (DSS) induced colitis in mice were assessed in this study. During a seven-day period of exposure to 3% DSS, sixty male BALB/c rodents were divided into six groups (n=10 per group) and administered MTK at doses of 50, 100, or 200 mg/kg/day. Animals were randomly selected within each group for subset analyses, regardless of disease severity or treatment response. In the CON, MOD, and MTK-H (200 mg/kg/day) groups, histological analyses were undertaken on six mice per group (n=6), while 16S rRNA sequencing and untargeted metabolomics were conducted on three mice per group (n=3). The data were analyzed using one-way ANOVA, followed by Tukey's test or the appropriate nonparametric test. MTK decreased disease activity, body weight loss, and colon shortening, increased IL-10 and SOD, and decreased TNF-α, IL-6, MPO, and MDA ($P<0.05$). MTK also enhanced the expression of ZO-1, Occludin, and Claudin-3, as well as the PAS-positive area and colonic histopathology. This was accompanied by an increase in the expression of Nrf2 and HO-1 proteins, as well as a decrease in the p-p65/p65 and p-IκBα/IκBα ratios. MTK-associated changes in gut microbial composition and faecal metabolites related to amino acid, bile acid, lipid, and tryptophan/indole metabolism were identified through multi-omics analyses. Additionally, associations among microbial, metabolic, inflammatory, oxidative, and barrier-related variables were identified through integrated analyses. These discoveries substantiate the intestinal protective effectiveness of MTK and establish a foundation for additional mechanistic and veterinary investigations.

To Cite This Article: Li Y, Yang Q, Ren H, Wang H, Fan B, Xia Z, Xu W, Deng Q, Fan F, Huang L, Wu J and Liao W, 2026. *Malus toringoides* polysaccharide alleviates dss-induced colitis in mice and is associated with gut microbiota–metabolite remodeling and Nrf2/HO-1–NF-κB signaling. Pak Vet J, 46(8): 1945-1957. http://dx.doi.org/10.29261/pakvetj/2026.196

INTRODUCTION

Intestinal inflammatory diseases are common disorders affecting both humans and animals and are characterized by persistent intestinal inflammation, epithelial barrier dysfunction, oxidative stress, and gut microbial dysbiosis. In veterinary medicine, enteric inflammatory diseases frequently occur in livestock, poultry, companion animals, and experimental animals, leading to diarrhea, impaired nutrient absorption, growth retardation, reduced feed efficiency, and increased susceptibility to secondary infections, thereby causing

considerable economic losses to the animal industry (Pluske *et al.*, 2018; Gresse *et al.*, 2017; Travis *et al.* 2024). In production animals, enteric inflammation triggered by pathogens, weaning, dietary factors, or environmental stress can impair epithelial barrier function and disturb microbial balance, thereby adversely affecting health and productive performance (Awad *et al.*, 2017; Tang *et al.*, 2025). The DSS induced mouse model reproduces several key features of intestinal inflammatory injury, including mucosal damage, oxidative stress, inflammatory responses, barrier impairment, and microbial dysbiosis. Because similar pathological changes occur in veterinary enteric disorders, this model provides a useful experimental system for evaluating potential interventions targeting intestinal inflammation (Kiesler *et al.*, 2015; Upadhaya and Kim, 2021).

Redox imbalance is an important pathological feature of ulcerative colitis. In DSS induced intestinal injury, excessive ROS production promotes lipid peroxidation, increases MDA levels, and impairs endogenous antioxidant defenses, including SOD, GSH-Px, and T-AOC (Tian *et al.*, 2017; Guo *et al.*, 2022; Travis *et al.*, 2024). Tight junction disruption and decreased expression of barrier-related proteins including ZO-1, Occludin, and Claudin-3 can result from persistent oxidative stress, which can worsen mucosal inflammation and epithelium damage. While NF-κB is essential for controlling inflammatory genes, the Nrf2/HO-1 pathway is a significant part of the cellular antioxidant response (Li *et al.*, 2024). Regulation of the Nrf2/HO-1–NF-κB axis has been suggested as a possible tactic for reducing oxidative damage and inflammation while maintaining epithelial barrier integrity in ulcerative colitis due to the functional interaction between these signalling pathways (Wardyn *et al.*, 2015; Wang *et al.*, 2022; Shu *et al.*, 2024; Li *et al.*, 2025).

Natural polysaccharides, as a significant category of food-derived bioactive macromolecules, have garnered substantial interest for their possible role in intestinal health management. In contrast to traditional pharmacological drugs, polysaccharides typically perform their biological roles via indirect and multitarget interactions with the gut ecology. Not enough digestion in the upper gastrointestinal tract means a lot of plant polysaccharides end up in the colon. There, they are fermented by microbes. Short-chain fatty acids, bile acids, amino acid derivatives, tryptophan-derived indoles, and lipid mediators are among the microbial metabolites that can be produced as a result of these modifications (Makki *et al.*, 2018; Bi *et al.*, 2025). These metabolites operate as crucial signalling molecules that control host-microbiota balance, oxidative stress reactions, mucosal immunology, and epithelial barrier function. A growing body of research indicates that plant-derived polysaccharides can reduce experimental colitis by changing the metabolic activity and composition of gut microbes, reducing inflammatory reactions, and strengthening the integrity of the intestinal barrier.

Malus toringoides (Rehd.) Hughes is a medicinal plant mainly distributed in the high-altitude regions of western China, particularly in Ganzi Prefecture, Sichuan Province. A regional phytochemical survey of E'seguo fruits collected from 12 areas of Ganzi showed that M. toringoides is more widely distributed than M. transitoria and contains a relatively high total polysaccharide content, averaging approximately 24.92%, with marked regional variation (Jiang *et al.*, 2024). This evidence supports polysaccharides as an important constituent of *M. toringoides* fruits. However, previous pharmacological studies on this species have mainly focused on non-polysaccharide fractions. For example, flavonoids isolated from M. toringoides leaves exhibited hypoglycemic activity in diabetic mice and rats and were accompanied by increased hepatic SOD activity and reduced MDA levels (Li *et al.*, 2014). More recently, phloridzin derivatives isolated from M. toringoides leaves also showed antioxidant activity in zebrafish and in vitro antioxidant assays (Liu *et al.*, 2026). These studies demonstrate the broader biological potential of M. toringoides but cannot be directly extrapolated to its fruit-derived polysaccharide fraction. Therefore, the effects of M. toringoides fruit polysaccharide (MTK) on intestinal inflammatory injury, gut microbial composition, and metabolic homeostasis remain insufficiently characterized.

This work thoroughly evaluated the intestinal health-promoting potential of *M. toringoides* polysaccharide (MTK) by investigating its protective effects in a DSS induced colitis mouse model. The study evaluated intestinal inflammatory responses, oxidative stress, mucosal barrier integrity, gut microbial composition, and microbiota-associated metabolic alterations. The antioxidant and anti-inflammatory effects of MTK were investigated by further examining the changes in Nrf2/HO-1- and NF-κB-related proteins. These results offer experimental evidence of MTK's intestinal protective activity and encourage its further investigation as a natural polysaccharide candidate for the enhancement of intestinal health.

MATERIALS AND METHODS

Preparation and purification of *Malus toringoides* polysaccharide: *Malus toringoides* polysaccharide (MTK) was extracted from mature fruits collected in Ganzi, Sichuan Province, China. The dried fruits were ground into a powder and passed through a 60-mesh sieve. First, we treated the powder with absolute ethanol (1:10, w/v) at room temperature. This removed the lipid-soluble impurities. Then, we extracted the powder twice with distilled water (1:20, w/v) at 60°C for 4hrs. After that, we combined the extracts and concentrated them. We then precipitated the extracts overnight with four volumes of absolute ethanol. Finally, we separated the mixture using a centrifuge at 8,000×g for 10min. This gave us the crude polysaccharide. After a series of chemical steps, including the removal of proteins using enzymes, the extraction of chloroform/n-butanol and petroleum ether, the decolorization of AB-8 resin, and the dialysis using a 3-kDa membrane, the polysaccharide solution was made into a powder using ethanol, and then dried to obtain purified MTK. The total amount of carbohydrates was found using a method that involved the use of phenol and sulfuric acid. This amount increased from 44.4% in the original extract to 77.2% after purification.

Animals and experimental design: Beijing SPF Biotechnology Co., Ltd. provided sixty male SPF BALB/c mice that were six to eight weeks old. The Animal Ethics Committee of Yunnan Agricultural University accepted all experimental protocols (Approval No. APYNAU 202503089), and animals were kept in conventional laboratory conditions. The mice were divided into six groups (n=10/group) at random after a 7-day acclimatisation period: CON, MOD, PC, MTK-L, MTK-M, and MTK-H. As shown in Fig. 1A, all groups except CON were given 3% (w/v) dextran sulphate sodium (DSS; molecular weight 40 kDa; MP Biomedicals, Irvine, CA, USA) in the drinking water for seven days in a row to induce acute colitis. While mice in the MTK-L, MTK-M, and MTK-H groups were given oral MTK at 50, 100, and 200mg/kg/day, respectively, mice in the PC group were given 5-ASA at 100 mg/kg/day. Throughout the trial, daily measurements were made of body weight, faecal bleeding, and stool consistency. There were no exclusions or fatalities. All animals were included in the general clinical assessment, while animals for endpoint-specific subset analyses were randomly selected within each group as described below.

Disease activity index and sample collection: The clinical severity was assessed on a daily basis using the disease activity index (DAI), a composite score that is derived from faecal haemorrhage, stool consistency, and body weight loss. The weight reduction was graded from 0 to 4 (0: no loss, 1: 1–5%, 2: 5–10%, 3: 10–20%, 4: >20%), the stool form was scored from 0 (normal), 2 (loose), or 4 (diarrhoea), and the faecal blood was scored from 0 (negative), 2 (occult blood), or 4 (gross haemorrhage) (Kim *et al.*, 2012). In order to collect blood from the retro-orbital venous plexus, animals were anaesthetised with isoflurane (3–4% induction, 1.5–2.5% maintenance) at the experimental endpoint. Cervical dislocation was carried out right away after the serum was separated by centrifugation at 3,000×g for 10 minutes at 4°C. After removing the whole colon—from the cecal junction to the anus—it was gently flushed with ice-cold PBS, lay flat without being stretched, and its length was measured. Colonic tissues were then obtained for molecular, biochemical, and histopathological analyses.

Histological analysis and intestinal barrier assessment: The colonic specimens were paraffin-embedded, fixed in 4% paraformaldehyde, and cut into 5μm sections. Hematoxylin eosin (HE) staining was implemented to evaluate histological morphology, while periodic acid–Schiff (PAS) staining was implemented to evaluate the integrity of the mucous barrier and the abundance of goblet cells. The histopathological damage was scored in a blinded manner in accordance with Kim *et al.* (2012), which included crypt architecture (0–3), inflammatory infiltration (0–3), muscular thickening (0–3), goblet cell loss (0–1), and crypt abscesses (0–1). The sum of these sub-scores was a total score of 0–11, with higher values indicating more severe injury. To represent each animal, three random non-overlapping fields were examined and averaged for each section. The PAS-positive area was quantified in ImageJ as the percentage of the stained region relative to the total tissue area, with three fields per section being captured under uniform imaging settings. The fluorescence intensity of three arbitrarily acquired fields per section was quantified in ImageJ using consistent parameters, with the field average representing each animal. Immunofluorescence staining was conducted for the tight junction proteins ZO-1, Occludin, and Claudin-3. Six biological replicates were included in each group (n=6) for all histological, PAS, and immunofluorescence analyses.

Determination of inflammatory cytokines and oxidative stress markers: Commercial ELISA kits from Multi Sciences (Hangzhou, China) were used to measure the quantities of IL-6 (Cat. No. EK206), TNF-α (Cat. No. EK282HS), and IL-10 (Cat. No. EK210) in colonic tissues. Assay kits from Solarbio (Beijing, China) were used to measure colonic SOD activity (Cat. No. BC5165), MDA content (Cat. No. BC0025), and MPO activity (Cat. No. BC5715) in accordance with the manufacturers' instructions.

Western blot analysis: To homogenise frozen colonic specimens, protease and phosphatase inhibitors were added to the RIPA lysis solution. After centrifugation at 12,000×g for 15 minutes at 4°C, the protein contents in the supernatants were measured using the BCA assay. Equal amounts of protein (20μg per lane) were separated using 10% SDS-PAGE and electrotransferred onto PVDF membranes. Membranes were blocked with 5% nonfat milk and then incubated overnight at 4 °C with primary antibodies against Nrf2 (Cat. No. 16396-1-AP, 1:5,000), HO-1 (Cat. No. 10701-1-AP, 1:10,000), NF-κB p65 (Cat. No. 80979-1-RR, 1:5,000), IκBα (Cat. No. 10268-1-AP, 1:15000), and phospho-IκBα (Cat. No. 82349-1-RRRRRRR, 1:5,000). After that, membranes were cleaned and probed for two hours at room temperature using HRP-conjugated secondary antibody (Proteintech; Cat. No. RGAR001; 1:5,000). NF-κB p65 and IκBα phosphorylation were represented as the p-p65/p65 and p-IκBα/IκBα ratios, respectively, while Nrf2 and HO-1 levels were normalized to GAPDH. Immunoreactive bands were visualized by enhanced chemiluminescence and densitometrically quantified using ImageJ.

Gut microbiota analysis: Stool samples and colonic luminal contents from the CON, MOD, and MTK-H (200 mg/kg/day) groups were taken under sterile conditions and kept at -80 °C until analysis. Each group (n=3) utilized three copies of the bacterial 16S rRNA gene. A commercially available kit was used to extract total microbial genomic DNA, and NanoDrop spectrophotometry and agarose gel electrophoresis were used to assess the DNA's purity and amount. Using primers 338F (5′-ACTCCTACGGGAGGCAGCAG-3′) and 806R (5′-GGACTACHVGGGTWTCTAAT-3′), PCR amplification focused on the V3-V4 hypervariable region (Mori *et al.*, 2014). After purification, amplicons were measured, mixed at equivalent molar ratios, and then paired-end sequenced using an Illumina NextSeq 2000 device. Amplicon sequence variations (ASVs) were produced by downstream processing using quality trimming with fastp, read merging with FLASH, and denoising with DADA2 implemented in QIIME2.

Alignment with the SILVA reference database was used to assign taxonomy. Good's coverage estimate and rarity analysis were employed to verify adequate sequencing depth. Beta diversity was visualised using principal coordinate analysis (PCoA) based on Bray Curtis distances, while alpha diversity was quantified using Sobs, Chao1, Shannon, and Simpson indices. LEfSe was employed to identify discriminative taxa (LDA threshold >2.0, $P<0.05$), and PERMANOVA and ANOSIM were employed to identify statistical differences in community composition.

Untargeted metabolomics analysis: Faecal metabolomic profiling was conducted for the CON, MOD, and MTK-H groups using three distinct biological replicates for each group (n=3). The supernatants were analysed using a UHPLC system connected to an Orbitrap Exploris 240 mass spectrometer (Thermo Scientific, USA) after metabolites were extracted under cool conditions and centrifuged at 13,000 × g for 15 minutes at 4°C. In order to monitor analytical stability, pooled QC samples were generated by combining equal proportions of each individual sample and injecting them at regular intervals throughout the cycle. Progenesis QI (version 3.0, Waters, USA) was used on the Majorbio Cloud Platform to process raw spectral data for peak detection, alignment, normalisation, and metabolite annotation. Compound identification was accomplished by comparing MS/MS fragmentation patterns with the HMDB and METLIN databases.Principal component analysis (PCA) was employed to investigate global metabolic variation and QC clustering, while partial least-squares discriminant analysis (PLS-DA) was employed to evaluate intergroup differences. Further evaluation of model performance and potential overfitting was conducted through 200 permutation tests, with R^2 and Q^2 representing predictive ability and goodness of fit, respectively. The identification of differential metabolites was conducted using variable importance in projection (VIP) >1 and Benjamini Hochberg FDR adjusted $P<0.05$, followed by KEGG pathway enrichment analysis.

Multi-omics integration analysis: Integrated exploratory analyses were conducted to characterize relationships among microbial features, differential metabolites, and host-associated parameters. Redundancy analysis (RDA) was applied to examine associations between selected bacterial genera and phenotypic, inflammatory, oxidative stress, and intestinal barrier indices. Using Pearson correlation analysis, associations between important genera and typical differential metabolites were further assessed; a high connection was defined as $|r| > 0.6$. Relationships between microbial profiles, metabolomic characteristics, host factors, and proteins linked to Nrf2/HO-1–NF-κB signalling were investigated using Mantel testing. The Benjamini-Hochberg false discovery rate approach was used to modify P values for multiple comparison analyses, and adjusted $P<0.05$ was deemed significant.

Statistical analysis: The mean±standard deviation (SD) is used to display the findings. R and GraphPad Prism were used to conduct statistical analysis. Group differences were assessed using a one-way ANOVA followed by Tukey's multiple-comparison test or, when appropriate, the Kruskal-Wallis test followed by Dunn's post hoc test, depending on the distributional features of the data. $P<0.05$ was set as the cutoff point for statistical significance.

RESULTS

MTK ameliorated DSS induced colitis symptoms, inflammatory responses, and oxidative stress injury in mice: Compared to the CON group, the DSS treatment induced the typical manifestations of colitis, including increased DAI scores, body weight loss, and colon shortening. MTK treatment reduced DAI scores, attenuated body weight loss, and partially restored colon length, with the MTK-H group showing the largest numerical improvement among the MTK-treated groups (Fig. 1B–E). DSS exposure significantly increased colonic TNF-α and IL-6 levels and decreased IL-10 levels compared with the CON group ($P<0.01$), indicating a marked inflammatory response. MTK treatment decreased TNF-α and IL-6 levels and increased IL-10 levels compared with the MOD group, with greater numerical changes observed in the MTK-H group (Fig. 1F–H). Similarly, DSS significantly reduced SOD activity and increased MPO activity and MDA levels ($P<0.01$), consistent with impaired antioxidant capacity, inflammatory activity, and lipid peroxidation. MTK treatment increased SOD activity and reduced MPO activity and MDA levels, with the magnitude of these numerical changes generally increasing across the MTK treatment groups (Fig. 1I–K). Collectively, these findings indicate that MTK alleviated DSS-induced clinical manifestations and was associated with improvements in inflammatory and oxidative stress-related indicators.

MTK ameliorated DSS induced colonic histopathological injury and restored intestinal mucosal barrier integrity: DSS caused significant colonic histological damage, as seen by H&E staining. This damage included mucosal disruption, crypt loss and deformation, epithelial destruction, and widespread infiltration of inflammatory cells. Following MTK therapy, these degenerative changes were reduced; the MTK-H group showed the greatest improvement (Fig. 2A). The histopathological score of the MOD group was substantially higher than that of the CON group ($P<0.01$), which was consistent with the histological findings. Conversely, the 5 ASA and all MTK interventions significantly reduced the score when compared to the MOD group ($P<0.01$). Of the MTK-treated groups, the MTK-H group had the lowest score (Fig. 2D). Additionally, PAS staining revealed a significant decrease in PAS positive goblet cells in the MOD group, suggesting mucus barrier degradation. The PAS positive area grew as a result of MTK therapy, with the MTK-H group showing the largest increase ($P<0.01$) (Fig. 2B, E). DSS decreased the fluorescence intensity and interfered with the distribution of Claudin-3, Occludin, and ZO-1 along the colonic epithelium, according to immunofluorescence studies. These tight

junction proteins' fluorescence intensities were raised by MTK treatment, with the MTK-H group showing the most alterations (Fig. 2C, F–H). All of these results show that MTK was linked to better mucus barrier and tight junction integrity and reduced DSS induced colonic histopathology damage.

MTK modulated the Nrf2/HO-1–NF-κB axis to alleviate DSS induced oxidative stress and inflammatory signaling activation: The MOD group exhibited a significant decrease in HO-1 and Nrf2 protein levels in comparison to the CON group ($p<0.01$), suggesting that the antioxidant defence was compromised following DSS exposure. In contrast, the expression of HO-1 and Nrf2 was increased to varying degrees in the PC and MTK-treated cohorts, with the MTK-M and MTK-H groups exhibiting more substantial effects ($P<0.01$) (Fig. 3A–C).

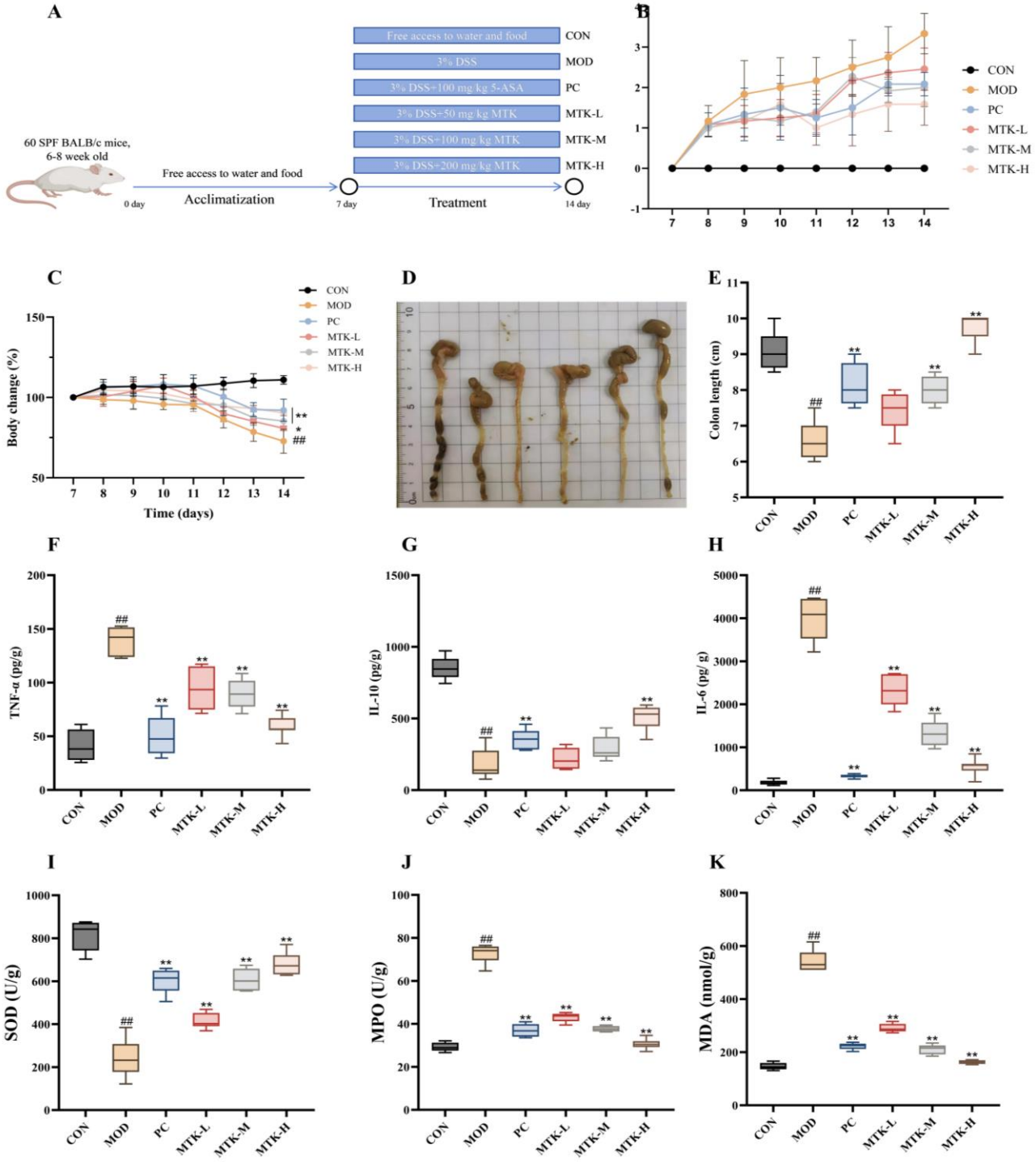

Fig. 1: Effects of MTK on clinical manifestations, inflammatory responses, and oxidative stress in DSS induced colitis mice. (A) Schematic overview of the experimental design. After 7 days of acclimation, mice were assigned to CON, MOD, PC, MTK-L, MTK-M, or MTK-H groups. Except for CON, all mice were exposed to 3% DSS for 7 days. The PC group received 5-ASA (100mg/kg/day), and MTK was administered at 50, 100, and 200mg/kg/day in the low, medium, and high dose groups, respectively. (B) DAI scores during the experimental period. (C) Changes in body weight. (D) Representative colon images. (E) Colon length. (F–H) TNF-α, IL-10, and IL-6 levels in colonic tissue. (I–K) SOD activity, MPO activity, and MDA content. Data are presented as mean±SD. $P<0.01$ versus CON; *$P<0.05$ and **$P<0.01$ versus MOD.

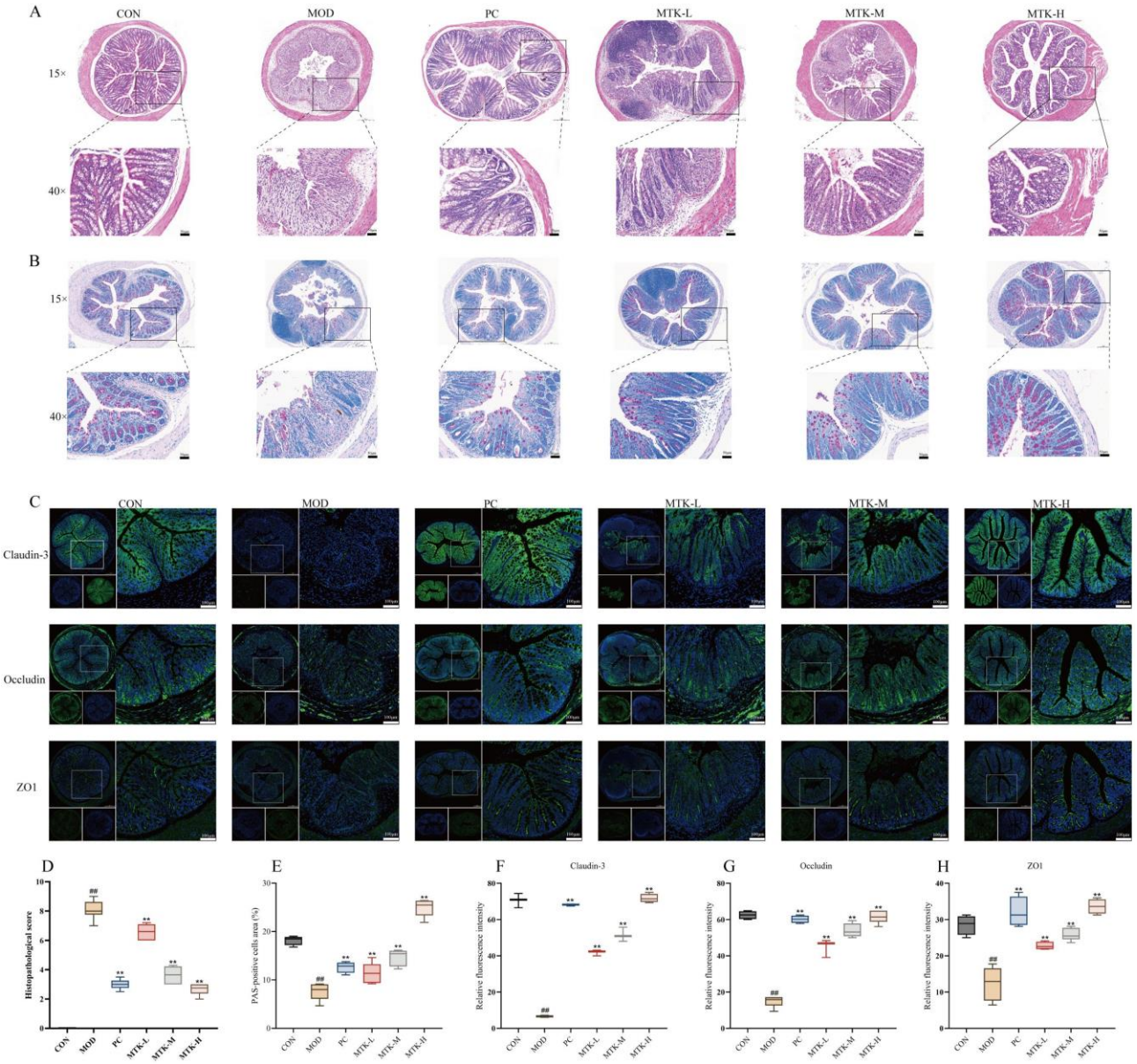

Fig. 2: Effects of MTK on colonic histopathology, mucus barrier, and tight junction proteins in DSS induced colitis mice. (A) Representative HE stained colon sections showing histopathological changes (scale bar=50μm). (B) PAS staining of goblet cells and mucus associated structures (scale bar=60μm). (C) Immunofluorescence staining of Claudin-3, Occludin, and ZO-1, with target proteins shown in green and DAPI stained nuclei in blue (scale bar=100 μm). (D) Blinded histopathological injury scores. (E) PAS-positive area expressed as a percentage of total tissue area. (F–H) Relative fluorescence intensities of Claudin-3, Occludin, and ZO-1, respectively. Three randomly selected non overlapping fields were analyzed per section using six independent biological samples per group (n=6). Data are presented as mean±SD. P<0.01 versus CON; *P<0.05 and **P<0.01 versus MOD.

The p-p65/p65 and p-IκBα/The MOD group exhibited a significant increase in IκBα ratios in comparison to the CON group (P<0.01), which is consistent with the enhancement of NF-κB signalling. The MTK treatment resulted in a reduction of both ratios, with the MTK-H group exhibiting the most significant changes (P<0.01), particularly for p-IκBα/IκBα (Fig. 3D–F). In general, MTK treatment was linked to reduced phosphorylation of NF-κB pathway related proteins and increased Nrf2 and HO-1 protein expression in DSS induced colitis rodents.

MTK reshaped the gut microbial structure in DSS induced colitis mice: 16S rRNA sequencing was conducted to assess the impact of MTK on gut microbiota in mice with DSS induced colitis. Rarefaction curves attained a plateau, signifying enough sequencing depth for diversity assessment (Fig. 4A). Alpha diversity study indicated that DSS modified gut microbial diversity, as seen by alterations in the Simpson, Shannon, Sobs, and Chao1 indices. The MTK intervention elevated the Sobs and Chao1 indices and indicated a rising trend in the Shannon index, implying improved microbial richness and diversity (Fig. 4B–E). PCoA analysis demonstrated distinct separation among the CON, MOD, and MTK groups, indicating substantial variations in microbial community structure (R=1.000, P=0.001). The MOD group was differentiated from the CON group, but the MTK group constituted a separate cluster from the MOD group, suggesting that MTK altered DSS disrupted gut microbiota (Fig. 4F). Taxonomic analysis showed that Bacillota, Bacteroidota, Actinomycetota, Pseudomonadota, Thermodesulfobacteriota, and Campylobacterota were the dominant phyla (Fig. 4G). At the genus level, DSS increased the relative abundance of

Bacteroides, Helicobacter, and norank_f__Desulfovibrionaceae, whereas MTK reduced these taxa and increased Christensenellaceae_R-7_group, Adlercreutzia, and Romboutsia (Fig. 4H). LEfSe analysis further confirmed that Bacteroides, Helicobacter, Desulfovibrionaceae, and Campylobacterota related taxa were enriched in the MOD group, whereas Christensenellaceae_R-7_group, Adlercreutzia, and Romboutsia were enriched in the MTK group (Fig. 4I, J). Further comparison of key genera showed that norank_f__Desulfovibrionaceae, Bacteroides, and Helicobacter were significantly increased in the MOD group but decreased after MTK intervention, while Christensenellaceae_R-7_group and Adlercreutzia increased after MTK treatment (Fig. 4K–P). Overall, MTK reshaped the gut microbial structure in DSS induced colitis mice by reducing model associated taxa and increasing potential metabolism associated taxa, providing microbial evidence for its intestinal protective effects.

MTK reshaped the fecal metabolic profile in DSS induced colitis mice: In order to identify variations in faecal metabolic profiles between the groups, untargeted metabolomics was implemented. The cumulative R^2X, R^2Y, and Q^2 values of the CON, MOD, and MTK-H groups were 0.789, 0.998, and 0.927, respectively, in PLS-DA (Fig. 5A). These values indicated an evident separation. The model was further evaluated using 200 permutation tests. Venn analysis identified 381 metabolites shared among the three groups, together with group specific metabolites, indicating differences in metabolite composition (Fig. 5B). Hierarchical clustering further showed distinct metabolic patterns among the CON, MOD, and MTKgroups, with the MTK-H group displaying a metabolic profile different from that of the MOD group (Fig. 5C). Pearson correlation analysis of representative differential metabolites revealed multiple positive and negative associations, suggesting coordinated changes among these metabolites following DSS exposure and MTK treatment (Fig. 5D).

VIP analysis revealed the differentially abundant metabolites that contributed most to the separation between the MTK and MOD groups, including biliverdin, 3,7-dihydroxy-12-oxocholanoic acid, fructosyl lysine, Arg-Pro, L-lysine, and several metabolites related to lipid, bile acid, and indole metabolism (Fig. 5E). Subsequent examination of typical differentially abundant metabolites indicated that MTK markedly elevated the concentrations of amino acids and associated metabolites, such as L-lysine, L-tyrosine, L-valine, L-proline, citrulline, and fructosyl-lysine (Fig. 5F). In addition, the levels of metabolites associated with redox regulation and sulfur containing metabolism, such as biliverdin, S-ethyl-L-cysteine, N-acetyl-L-methionine, and taurine, increased in the MTK group (Fig. 5G). LPC, PC, LPE, prostaglandin F2α, 19(R)-hydroxy prostaglandin A2, 3,7-dihydroxy-12-oxocholanoic acid, 7-ketodeoxycholic acid, taurodeoxycholic acid, indole-3-lactic acid, indole-3-carboxylic acid, and trans-3-indoleacrylic acid are among the metabolites associated with lipid metabolism, bile acid metabolism, and tryptophan/indole metabolism (Fig. 5H–J).

The differential metabolites were primarily involved in the following processes: aminoacyl tRNA biosynthesis, protein digestion and absorption, alanine, aspartate, and glutamate metabolism, arginine biosynthesis, glycerophospholipid metabolism, D-amino acid metabolism, arachidonic acid metabolism, cholesterol metabolism, bile secretion, primary bile acid biosynthesis, and purine and pyrimidine metabolism (Fig. 5K). This was illustrated by the KEGG enrichment analysis. In general, the faecal metabolic profile of DSS-induced colitis mice was significantly altered by MTK treatment, with a particular emphasis on amino acid, redox-related, lipid, bile acid, and tryptophan/indole-associated metabolites.

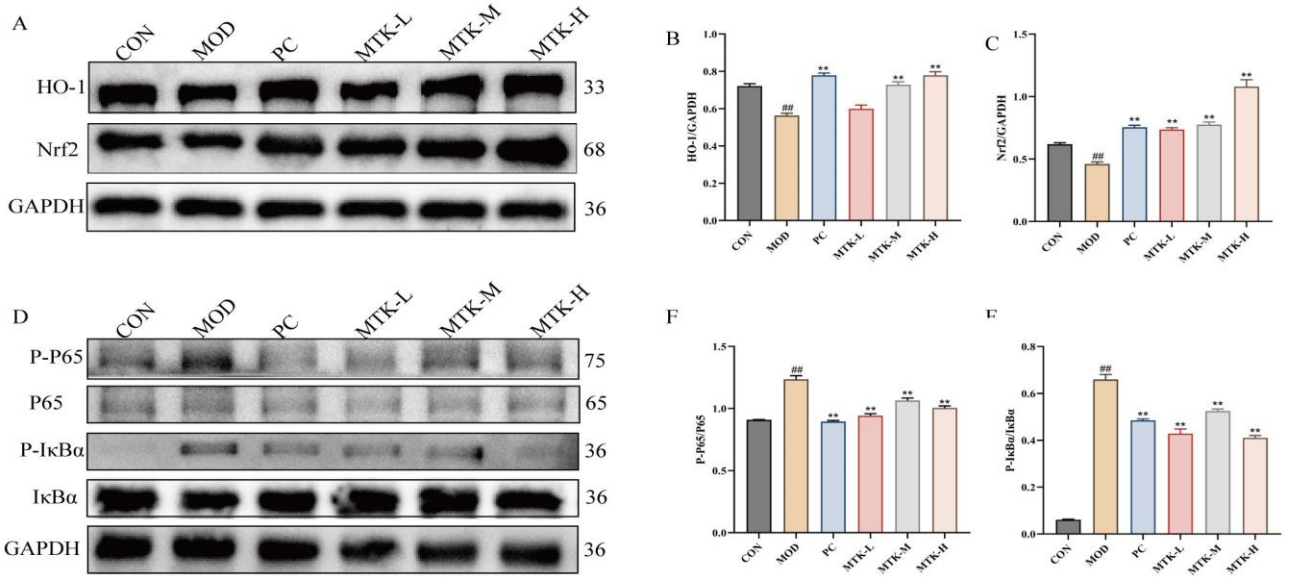

Fig. 3: Effects of MTK on Nrf2/HO-1 and NF-κB related protein expression in DSS induced colitis mice. (A) Representative immunoblots of HO-1, Nrf2, and GAPDH in colonic tissues. (B, C) Relative HO-1 and Nrf2 protein levels normalized to GAPDH. (D) Representative immunoblots of phosphorylated and total NF-κB p65 and IκBα. (E, F) Quantification of the p-p65/p65 and p-IκBα/IκBα ratios, respectively. Data are presented as mean±SD. P<0.01 versus CON; **P<0.01 versus MOD. CON, control; MOD, DSS model; PC, positive control; MTK-L/M/H, low, medium, and high dose MTK groups. GAPDH was used as the loading control.

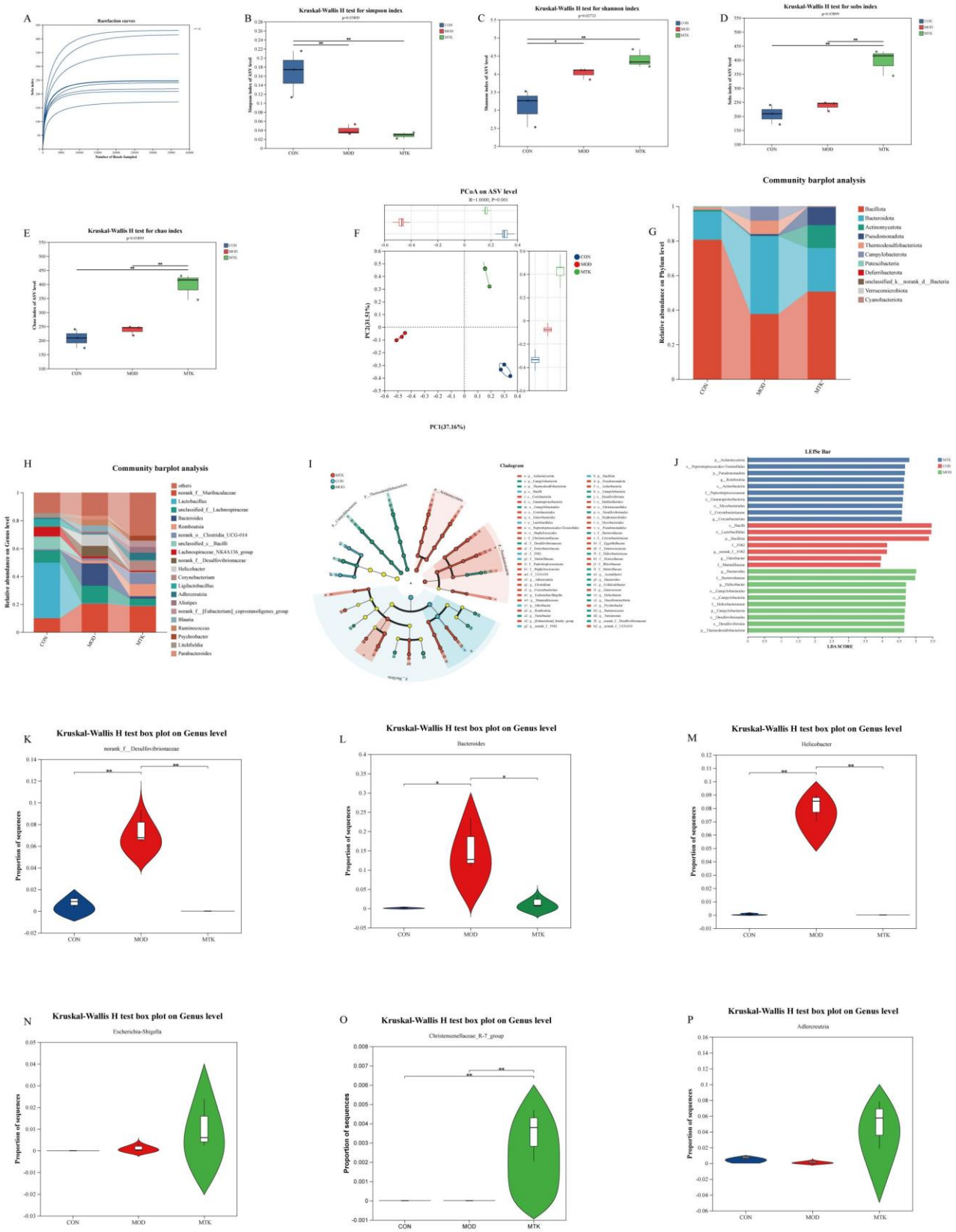

Fig. 4: MTK treatment was associated with alterations in gut microbial diversity, community structure, and taxonomic composition in DSS induced colitis mice. (A) Rarefaction curves based on ASV richness. (B–E) Alpha diversity indices, including Simpson, Shannon, Sobs, and Chao1. (F) Principal coordinate analysis (PCoA) based on Bray–Curtis distances showing differences in microbial community structure among the CON, MOD, and MTK-H groups. (G, H) Relative abundances of dominant bacterial taxa at the phylum and genus levels, respectively. (I) LEfSe cladogram showing differentially enriched taxa among groups. (J) LDA score distribution of discriminative taxa identified by LEfSe analysis. (K–P) Relative abundances of key differential genera, including norank_f__Desulfovibrionaceae, Bacteroides, Helicobacter, Escherichia-Shigella, Christensenellaceae_R-7_group, and Adlercreutzia. 16S rRNA sequencing was performed using three independent biological samples per group (n=3) from the CON, MOD, and MTK-H (200 mg/kg/day) groups. Alpha diversity indices and differential taxa were compared using the Kruskal–Wallis test followed by appropriate post hoc comparisons. LEfSe analysis was performed using an LDA score > 2.0 and P<0.05 as the significance threshold. *P<0.05 and **P<0.01; horizontal lines indicate the corresponding group comparisons. CON, control group; MOD, DSS model group; MTK-H, high dose MTK group.

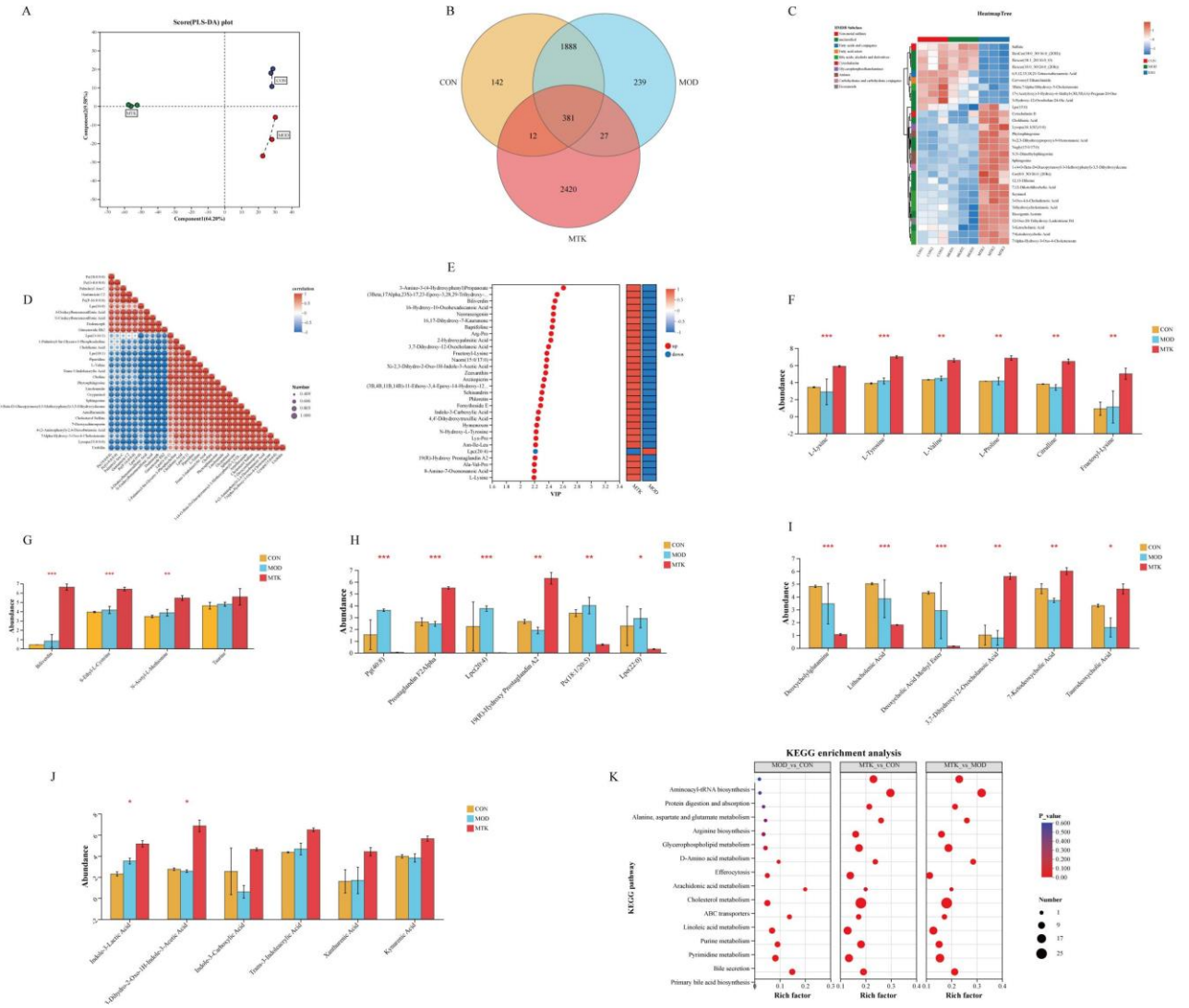

Fig. 5: Fecal metabolomic changes associated with MTK treatment in DSS induced colitis mice. (A) PLS-DA score plot illustrating metabolic profile differences among CON, MOD, and MTK-H. (B) Venn diagram of shared and group specific metabolites. (C) Hierarchical clustering heatmap, with red and blue representing relatively high and low abundance, respectively. (D) Pearson correlation matrix of selected differential metabolites; color indicates correlation direction and circle size reflects correlation strength. (E) VIP scores for metabolites differing between MTK-H and MOD, with red and blue indicating increased and decreased abundance, respectively. (F–J) Selected metabolites associated with amino acid, redox related, lipid, bile acid, and tryptophan/indole metabolism. (K) KEGG enrichment of differential metabolites for MOD versus CON, MTK-H versus CON, and MTK-H versus MOD; bubble size represents metabolite number and color indicates P value. Untargeted metabolomics was conducted using three independent biological samples per group (n=3) from CON, MOD, and MTK-H (200 mg/kg/day). Differential metabolites were defined by VIP > 1 and FDR adjusted P<0.05. CON, control; MOD, DSS model; MTK-H, high dose MTK.

Integrated analysis revealed close associations among MTK-mediated gut microbiota modulation, metabolic remodeling, oxidative stress attenuation, and barrier restoration: To further clarify the relationships among the gut microbiota, metabolites, and host responses under MTK intervention, RDA, Mantel tests, and Pearson correlation analysis were performed. RDA revealed clear separation among the CON, MOD, and MTK groups, indicating that both DSS modeling and MTK intervention altered the overall association pattern between the gut microbial structure and host indicators. The MOD samples were oriented mainly toward inflammatory and oxidative injury related indicators, including DAI, TNF-α, MDA, and MPO, whereas the MTK samples were closer to protective indicators such as SOD, colon length, and ZO-1. These results suggest that MTK-induced changes in gut microbial structure are closely associated with the alleviation of symptoms of colitis, increased antioxidant capacity, and improved barrier function. With respect to key bacterial genera, Bacteroides, norank_f__*Desulfovibrionaceae*, and Helicobacter were more closely associated with the MOD group and injury related indicators, whereas *Romboutsia*, *Christensenellaceae_R-7_group*, and *Adlercreutzia* tended to be associated with the improved phenotype after MTK intervention (Fig. 6A).

The Pearson correlation analysis demonstrated clear correlations between significant bacterial genera and distinctively abundant metabolites. *Adlercreutzia*, *Romboutsia*, and *Christensenellaceae_R-7_group* had a positive correlation with many metabolites, such as indole-3-carboxylic acid, biliverdin, indole-3-lactic acid, trans-3-indoleacrylic acid, taurodeoxycholic acid, 3,7-dihydroxy-12-oxocholanoic acid, L-lysine, and L-proline. Bacteroides, norank_f__Desulfovibrionaceae, and Helicobacter exhibited a negative correlation with some

indole derivatives, bile acid-related metabolites, and amino acid metabolites (Fig. 6B). The data indicate that MTK associated alterations in gut microbiota may be connected to modifications in tryptophan/indole metabolism, bile acid metabolism, amino acid metabolism, and metabolites related to antioxidants.

The results of the Mantel test and Pearson correlation analysis further supported the overall associations among the gut microbiota, metabolites, and host phenotypes and Helicobacter were strongly associated with injury related indicators, including DAI, TNF-α, IL-6, MDA, MPO, p-p65/p65, and p-IκB/IκB. In contrast, *Adlercreutzia, Christensenellaceae_R-7_group*, and *Romboutsia* were more closely associated with biliverdin, indole derivatives, bile acid related metabolites, L-lysine, L-proline, and protective indicators such as ZO-1, Occludin, Claudin-3, Nrf2, and HO-1 (Fig. 6C). The Pearson correlation analysis indicated that DAI, proinflammatory cytokine levels, oxidative stress markers, and NF-κB pathway phosphorylation levels exhibited positive correlations with one another, while demonstrating negative correlations with SOD activity, colon length, PAS positive area, tight junction protein expression, Nrf2/HO-1 expression, and the expression of various key metabolites. These findings indicate that microbial and metabolic alterations following MTK treatment were associated with changes in oxidative inflammatory status and intestinal barrier related indicators.

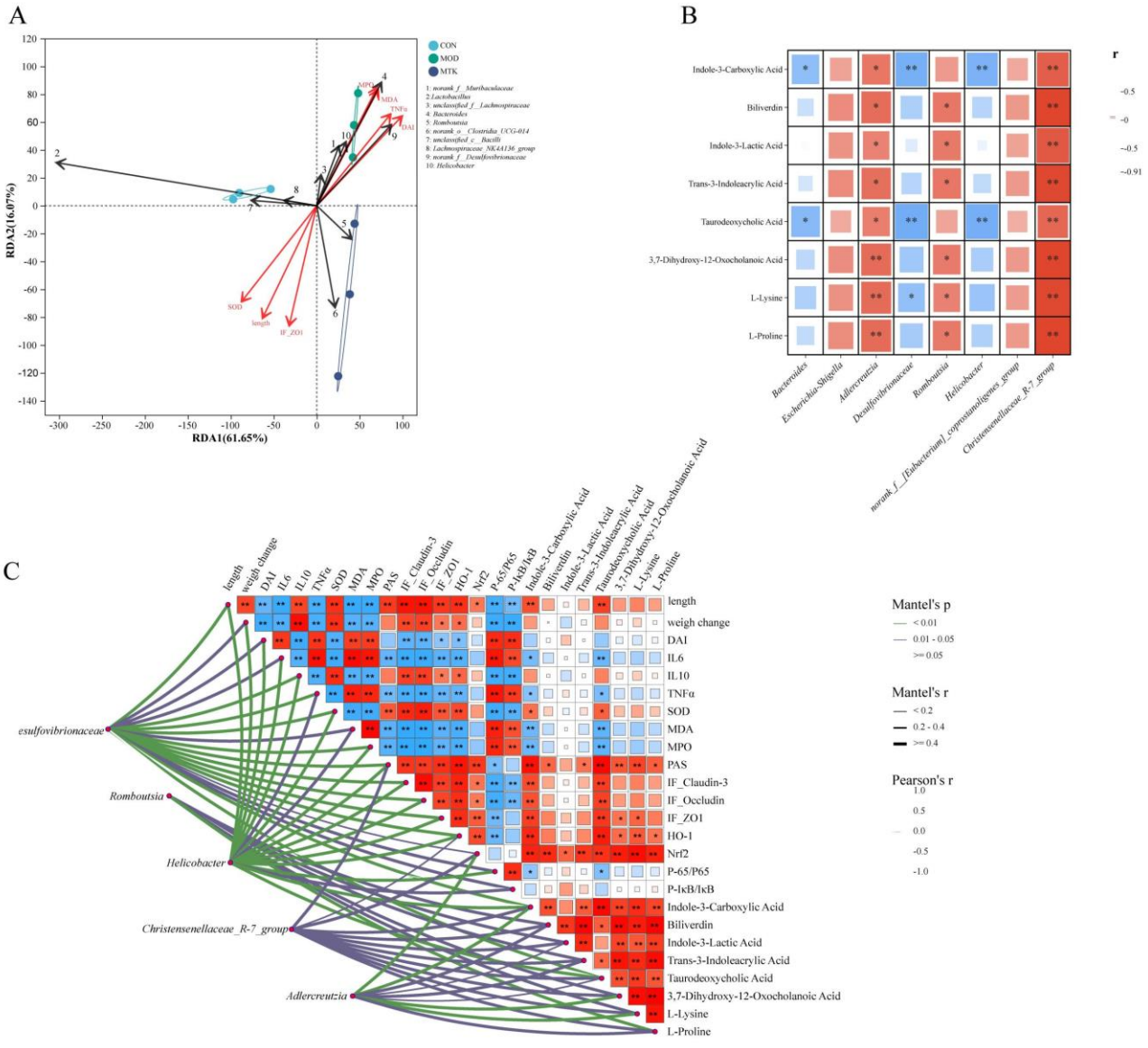

Fig. 6: Comprehensive correlation analysis among gut microbiota, fecal metabolites, and host associated markers. Redundancy analysis (RDA) illustrating the correlations among principal bacterial species, host phenotypic indicators, inflammatory and oxidative stress markers, and indices related to the intestinal barrier in the CON, MOD, and MTK groups. Black arrows denote bacterial species, whereas red arrows indicate host related markers, including DAI, TNF-α, MPO, MDA, SOD, colon length, and IF_ZO-1. The direction and length of the arrow signify the direction of correlation and the magnitude of contribution, respectively. Correlation heatmap illustrating the relationship between representative differential metabolites and principal bacterial genera. Red signifies positive correlations, whereas blue denotes negative correlations. (C) Mantel test and Pearson correlation network incorporating essential bacterial genera, host indicators, signaling pathway proteins, and representative metabolites. The heatmap color gradient illustrates Pearson's correlation coefficient, with red denoting positive correlations and blue signifying negative correlations. Connecting lines denote Mantel correlations between bacterial genera and host/metabolic factors; the color of the lines signifies Mantel's P value, while the breadth of the lines reflects Mantel's r value. *P<0.05 and **P<0.01. CON denotes the control group; MOD refers to the DSS model group; MTK indicates the MTK treated group; RDA signifies redundancy analysis.

DISCUSSION

Previous phytochemical studies have confirmed that M. toringoides fruits contain a substantial polysaccharide fraction, with regional analyses reporting relatively high total polysaccharide contents in fruits collected from Ganzi Prefecture (Jiang *et al.*, 2024). In contrast, most available pharmacological evidence for this species has focused on non polysaccharide fractions, particularly flavonoids and phloridzin related compounds derived from the leaves, which have shown antioxidant, hypoglycemic, and metabolic regulatory activities (Li *et al.*, 2014; Liu *et al.*, 2026). Therefore, these earlier findings demonstrate the broader biological potential of M. toringoides but do not directly define the biological activity of its fruit derived polysaccharide fraction. The present study extends this evidence by showing that a purified M. toringoides fruit polysaccharide preparation containing 77.2% total carbohydrate was associated with attenuation of DSS induced intestinal inflammatory injury.

DSS induced colonic injury is characterised by oxidative imbalance and inflammatory responses, which disrupt intestinal homeostasis. In the current study, the administration of DSS was associated with a significant oxidative inflammatory disturbance, as evidenced by the elevated levels of TNF-α, IL-6, MPO, and MDA, as well as the reductions in IL-10 and SOD. These modifications were substantially reversed by MTK treatment. MTK treated mice consistently exhibited increased Nrf2 and HO-1 protein expression, as well as decreased p-p65/p65 and p-IκBα/IκBα ratios. Nrf2/HO-1 is a critical endogenous antioxidant defence system, whereas NF-κB is a central regulator of inflammatory signalling in the intestine (Piechota Polanczyk A and Fichna, 2014; Ahmed *et al.*, 2017; Wang *et al.*, 2023; Zhang *et al.*, 2025). The coordinated changes in these proteins were consistent with the improvements in inflammation and oxidative parameters, indicating that the intestinal protective effects of MTK were linked to attenuated NF-κB related inflammatory signalling and strengthened antioxidant responses.

The attenuation of inflammatory and oxidative injury was accompanied by a marked improvement in intestinal barrier integrity. DSS caused extensive mucosal damage, loss of PAS positive goblet cells, and reduced expression of the tight junction proteins ZO-1, Occludin, and Claudin-3, indicating impairment of both the mucus and epithelial barriers. In contrast, MTK treatment preserved crypt architecture, increased goblet cell associated mucus secretion, and restored tight junction protein expression. These findings are consistent with the close relationship between the intestinal oxidative inflammatory environment and epithelial barrier integrity, as excessive oxidative stress and sustained inflammatory signaling can aggravate epithelial injury, disrupt tight junctions, and increase intestinal permeability (Suzuki, 2013; Odenwald and Turner, 2017; Chelakkot *et al.*, 2018). Taken together, the concurrent improvements in inflammatory and oxidative stress markers, signaling related proteins, and barrier associated indices suggest that MTK associated protection against acute DSS induced colonic injury involves closely linked improvements in the oxidative inflammatory environment and intestinal barrier integrity.

Changes in gut microbial composition may represent an important component associated with the intestinal protective effects of MTK. Food derived polysaccharides can serve as fermentable substrates for colonic microorganisms and exert prebiotic like regulatory effects (Xiang *et al.*, 2023; Wang *et al.*, 2025). 16S rRNA gene sequencing is a technique that is frequently employed to evaluate disease-associated dysbiosis and characterise intestinal microbial communities. However, it only provides indirect information on microbial functional potential and has limited taxonomic resolution (Shi *et al.*, 2024). Changes in gut microbial composition may represent an important component associated with the intestinal protective effects of MTK. In the present study, DSS markedly disturbed gut microbial composition, whereas MTK treatment reduced the relative abundance of model associated taxa, including *Desulfovibrionaceae*, *Helicobacter*, and *Bacteroides*, while increasing *Christensenellaceae_R-7_group*, *Adlercreutzia*, and *Romboutsia*. *Desulfovibrionaceae* and *Helicobacter* have been associated with inflammatory intestinal environments, whereas *Christensenellaceae_R-7_group* and *Adlercreutzia* are frequently linked to metabolic regulation and intestinal ecological homeostasis (Meng *et al.*, 2024; Yi *et al.*, 2025). These findings suggest that MTK treatment was accompanied by a shift in the gut microbial community toward a composition associated with improved intestinal homeostasis.

Untargeted metabolomics further revealed marked alterations in amino acid, bile acid, arachidonic acid, tryptophan/indole, and redox related metabolism following MTK treatment. Increased levels of L-lysine and L-proline may provide metabolic support for mucosal renewal and tissue repair, whereas changes in biliverdin and taurine were consistent with the improved antioxidant status observed in MTK treated mice. MTK also increased several indole derivatives, including indole-3-carboxylic acid. Such metabolites have been associated with AhR mediated regulation of epithelial barrier function and immune homeostasis (Roager and Licht, 2018). In addition, alterations in bile acid related metabolites, including taurodeoxycholic acid, suggest that bile acid metabolic remodeling may also be associated with the intestinal protective effects of MTK (Wahlström *et al.*, 2016). Collectively, these metabolic changes were consistent with the improvements in oxidative stress, inflammation, and intestinal barrier integrity observed after MTK treatment.

Integrated analyses further revealed close associations among gut microbial composition, fecal metabolites, and host phenotypes. RDA showed that MTK treated samples were more closely associated with protective indicators, including colon length, SOD activity, and tight junction protein expression, whereas MOD samples were associated with inflammatory and oxidative injury related variables. Pearson correlation analysis and Mantel tests further showed that MTK associated taxa, including *Adlercreutzia*, *Romboutsia,* and *Christensenellaceae_R-7_group*, were correlated with indole derivatives, bile acid related metabolites, amino acid metabolites, and barrier related indicators. These findings support coordinated microbial, metabolic, and

host responses following MTK treatment and provide a basis for further investigating their functional interactions. Because the present integrated analyses are association based, the specific causal relationships among these changes warrant further validation through microbiota depletion, fecal microbiota transplantation, targeted metabolite supplementation, and pathway inhibition studies.

Conclusions: In summary, *Malus toringoides* polysaccharide (MTK) attenuated acute DSS triggered colitis in mice, as demonstrated by reduced disease severity, ameliorated inflammatory and oxidative stress markers, restored colonic histological architecture, and enhanced mucus barrier and tight junction protein expression. These protective effects were paralleled by upregulated Nrf2 and HO-1 protein levels and diminished p-p65/p65 and p-IκBα/IκBα ratios. MTK administration also shifted gut microbial community structure and fecal metabolic profiles, with perturbations in amino acid, bile acid, lipid, redox, and tryptophan/indole metabolic pathways. Multi-omics integration further revealed correlations between microbial alterations, metabolic signatures, oxidative-inflammatory state, and intestinal barrier parameters. Collectively, these results offer preclinical support for the intestinal protective action of MTK in the acute DSS induced colitis model and lay the groundwork for subsequent mechanistic exploration.

Acknowledgment: We appreciate the assistance from our distinguished colleagues in the Department of Clinic Veterinary of Yunnan Agricultural University.

Funding: This article was supported by the Key Project of Sichuan Minzu College (Grant No. XYZB2505ZA) (Youying Li).

Conflict of interest: The authors have stated explicitly that there are no conflicts of interest in connection with this article.

Authors contribution: Youying Li and Qinhong Yang: Investigation, Data curation, Formal analysis, Writing – original draft, Visualization; Honghui Ren, Huikang Wang, Bin Fan and Zhaobin Xia: Methodology, Validation, Investigation, Resources, Software, Data curation; Wenbin Xu, Qian Deng and Feng Fan: reviewing & editing. Lishuxin Huang, Jianping Wu and Wenju Liao: Conceptualization, Funding acquisition, Project administration, Supervision, Writing – review & editing.

REFERENCES

Ahmed SM, Luo L, Namani A, *et al*., 2017. Nrf2 signaling pathway: pivotal roles in inflammation. Biochimica et Biophysica Acta–Molecular Basis of Disease 1863:585-597.

Awad WA, Hess C and Hess M, 2017. Enteric pathogens and their toxin-induced disruption of the intestinal barrier through alteration of tight junctions in chickens. Toxins 9:60.

Bi W, Sun J, Zhang Y, *et al*., 2025. Protective role of lotus leaf polysaccharides in mice with ulcerative colitis. Pakistan Veterinary Journal 45:1662-1673.

Chelakkot C, Ghim J and Ryu SH, 2018. Mechanisms regulating intestinal barrier integrity and its pathological implications. Experimental & Molecular Medicine 50:1-9.

Gresse R, Chaucheyras-Durand F, Fleury MA, *et al*., 2017. Gut microbiota dysbiosis in postweaning piglets: understanding the keys to health. Trends in Microbiology 25:851-873.

Guo H, Guo H, Xie Y, *et al*., 2022. Mo_3Se_4 nanoparticle with ROS scavenging and multi-enzyme activity for the treatment of DSS-induced colitis in mice. Redox Biology 56:102441.

Jiang M, Fan H, Chen Y, *et al*., 2024. Study on the bioactive constituent and mineral elements of the Tibetan medicine E'seguo from different regions of Ganzi Prefecture, China. Molecules 29:4154.

Kiesler P, Fuss IJ and Strober W, 2015. Experimental models of inflammatory bowel diseases. Cellular and Molecular Gastroenterology and Hepatology 1:154-170.

Kim JJ, Shajib MS, Manocha MM, *et al*., 2012. Investigating intestinal inflammation in the DSS-induced model of IBD. Journal of Visualized Experiments 60:e3678.

Li D, Peng C, Xie X, *et al*., 2014. Antidiabetic effect of flavonoids from *Malus toringoides* (Rehd.) Hughes leaves in diabetic mice and rats. Journal of Ethnopharmacology 153:561-567.

Li S, Lu S, Xiong J, *et al*., 2025. Hydroxyethyl starch-curcumin nanoparticles ameliorate DSS-induced ulcerative colitis in mice via synergistic TLR4/NF-κB suppression, Nrf2 activation, intestinal barrier restoration and gut microbiota modulation. Frontiers in Pharmacology 16:1610711.

Li Z, Wei C, Yang J, *et al*., 2024. High-fat intake induces gut microbiota disorders, inflammatory responses and oxidative stress in *Nyctereutes procyonoides*. Animal Diseases 4:27.

Liu L, Tian WW, Wang YC, *et al*., 2026. Three phloridzin derivatives capable of anti-oxidant from *Malus toringoides* (Rehd.) Hughes. Natural Product Research 40:1977-1982.

Makki K, Deehan EC, Walter J, *et al*., 2018. The impact of dietary fiber on gut microbiota in host health and disease. Cell Host & Microbe 23:705-715.

Meng A, Zhang X, Pubu P, *et al*., 2024. Protective effect of lentinan against LPS-induced injury in mice via influencing antioxidant enzyme activity, inflammatory pathways and gut microbiota. Pakistan Veterinary Journal 44:647-656.

Mori H, Maruyama F, Kato H, *et al*., 2014. Design and experimental application of a novel non-degenerate universal primer set that amplifies prokaryotic 16S rRNA genes with a low possibility of amplifying eukaryotic rRNA genes. DNA Research 21:217-227.

Odenwald MA and Turner JR, 2017. The intestinal epithelial barrier: a therapeutic target? Nature Reviews Gastroenterology & Hepatology 14:9-21.

Pluske JR, Turpin DL and Kim JC, 2018. Gastrointestinal tract (gut) health in the young pig. Animal Nutrition 4:187-196.

Roager HM and Licht TR, 2018. Microbial tryptophan catabolites in health and disease. Nature Communications 9:3294.

Shi Y, Peng G, Gebremariam AA, *et al*., 2024. Analytical insights, modulation and compositional dynamics of the feline gut microbiota: a review. Animal Diseases 4:36.

Shu L, Fu H, Pi A, *et al*., 2024. Protective effect of andrographolide against ulcerative colitis by activating the Nrf2/HO-1-mediated antioxidant response. Frontiers in Pharmacology 15:1424219.

Suzuki T, 2013. Regulation of intestinal epithelial permeability by tight junctions. Cellular and Molecular Life Sciences 70:631-659.

Tang X, Huang Y, Zhu Y, *et al*., 2025. Immune dysregulation in ulcerative colitis: pathogenic mechanisms and therapeutic strategies of traditional Chinese medicine. Frontiers in Cell and Developmental Biology 13:1610435.

Tian T, Wang Z and Zhang J, 2017. Pathomechanisms of oxidative stress in inflammatory bowel disease and potential antioxidant therapies. Oxidative Medicine and Cellular Longevity 2017:4535194.

Travis S, Bleakman AP, Dubinsky M, *et al*., 2024. The Communicating Needs and Features of IBD Experiences (CONFIDE) study: US and European patient and health care professional perceptions of the experience and impact of symptoms of moderate-to-severe ulcerative colitis. Inflammatory Bowel Diseases 30:939-949.

Upadhaya SD and Kim IH, 2021. The impact of weaning stress on gut health and the mechanistic aspects of several feed additives contributing to improved gut health function in weanling piglets—a review. Animals 11:2418.

Wahlström A, Sayin SI, Marschall HU, *et al*., 2016. Intestinal crosstalk between bile acids and microbiota and its impact on host metabolism. Cell Metabolism 24:41-50.

Wang K, Guo J, Chang X, *et al*., 2022. Painong-San extract alleviates dextran sulfate sodium-induced colitis in mice by modulating gut microbiota, restoring intestinal barrier function and attenuating TLR4/NF-κB signaling cascades. Journal of Pharmaceutical and Biomedical Analysis 209:114529.

Wang S, Wu P, Fan Z, *et al*., 2023. Dandelion polysaccharide treatment protects against dextran sodium sulfate-induced colitis by suppressing NF-κB/NLRP3 inflammasome-mediated inflammation and activating Nrf2 in mouse colon. Food Science & Nutrition 11:7271-7282.

Wang X, Yu C, Li Y, *et al*., 2025. Dietary polysaccharides as gut health regulators: structural characteristics and regulatory mechanism. Trends in Food Science & Technology 161:105074.

Wardyn JD, Ponsford AH and Sanderson CM, 2015. Dissecting molecular cross-talk between Nrf2 and NF-κB response pathways. Biochemical Society Transactions 43:621-626.

Xiang N, Zhao J, Chang S, *et al*., 2023. In vitro fecal fermentation of *Euphorbia humifusa*-derived polysaccharides and their protective effect against ulcerative colitis in mice. Foods 12:751.

Yi X, Lu W, Liu D, *et al*., 2025. Psyllium and inulin supplementation alleviates diarrhea and supports gut flora in pre-weaning calves. Pakistan Veterinary Journal 45:1061-1072.

Zhang L, Li T, Liu J, *et al*., 2025. The regulation of the NF-κB p65 and Nrf2/HO-1 signaling pathways by fucoxanthin in human THP-1 monocyte macrophages under a lipopolysaccharide-induced inflammation model. Foods 14:1746.